



NANOSCIENCE LABORATORY

HIGHLIGHTS 2014

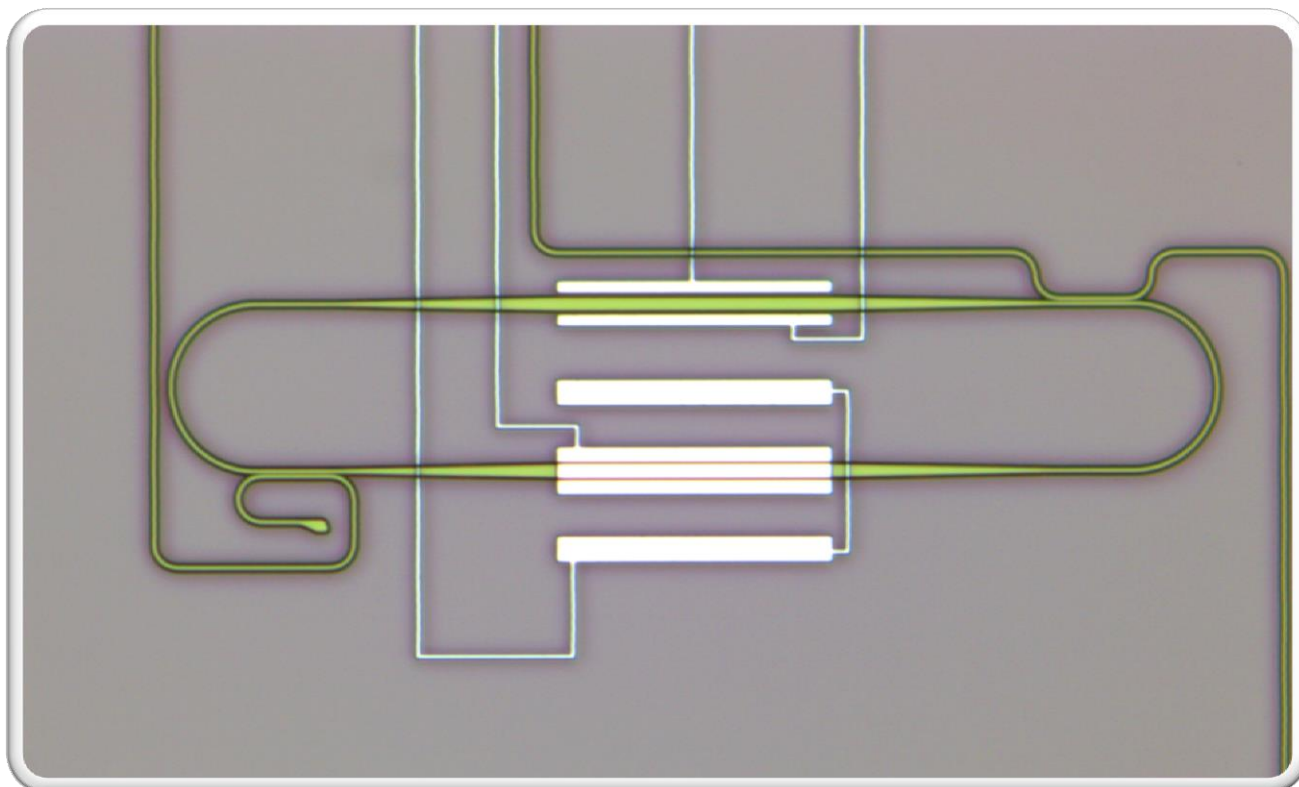


Image on the front cover:

An integrated Mach Zehnder fabricated in the FBK clean room,
Courtesy of Martino Bernard and of FBK



MEMBERS (2014)

Faculty and research staff

Lorenzo Pavesi (full professor, head)
Marina Scarpa (full professor)
Zeno Gaburro (associate professor)
Paolo Bettotti (researcher)
Fernando Ramiro Manzano (researcher)

Technical staff

Massimo Cazzanelli (EP2 level)
Enrico Moser
Giorgio Fontana (EP5 level)

Administrative staff

Tatsiana Yatskevich
Dina Shakirova (left September 2014)

Post-doctoral fellows

Mattia Mancinelli
Andrea Tengattini (left May 2014)
Romain Guider
Sanjay Thorat
Santanu Manna

Doctoral students

Davide Gandolfi
Massimo Borghi
Fabio Turri
Zahra Bisadi
Hafeez Ullah (left October 2014)
Stefano Tondini
Alessandro Trenti
Tatevik Chalyan

Master students

Anna Lion
Marta Guarisco
Johanna Mae Indias
Cecilia Maestri
Stefano Vidotto
Martino Bernard
Allegra Calabrese
Daniela Scardi
Stefano Biasi

SCIENTIFIC MISSION

Introduction to the Nanoscience Laboratory

The Nanoscience Laboratory (NL) is one of the scientific groups of the Department of Physics, University of Trento. Its main area of research are nanophotonics, silicon-based photonics and nanobiotechnologies. The mission of NL is to generate new knowledge, to develop understanding and to spin-off applications from physical phenomena associated with photons and low dimensional systems. In particular, NL works on applying the nanoscience paradigm to silicon or silicon compatible materials to develop micro and nanosystems compatible with the main driving silicon microelectronics technologies. However, silicon is not the only material studied. Other field of interest concerns the use of polymers to tailor the properties of nanostructure atom-by-atom or the use of metals to investigate new properties which rise from plasmonics. In addition, a particular emphasis is placed on quantum photonics and its applications.

NL research group consists of more than 20 people with

different scientific background. Such, researchers from physics, bio-chemistry, materials science and electrical engineering are gathered to form a group of interdisciplinary nature.

It is worth mentioning that NL collaborates closely with the Center of Materials and Microsystems, Fondazione Bruno Kessler (FBK). This collaboration spans over the last twenty years and covers such topics as fabrication, testing and application of biomaterials and silicon based devices. There are many common projects in which both parties participate. The current ones are: project "On silicon chip quantum optics for quantum computing and secure communications – SiQuero" (financed by the Province of Trento (PAT)) and the project "Integrated SYstem based on PHOtonic Microresonators and Microfluidic Components for rapid detection of toxins in milk and dairy products – SYMPHONY" (financed by the European Commission within the 7th framework). A new tight collaboration started with the Trento units of CNR-INO, specifically dedicated to implement quantum optics in a silicon integrated chip.

Moreover, with the support of FBK and CNR, every two years NL organizes a winter school on optoelectronics and photonics. The next edition will be the "8th Optoelectronics and Photonics Winter School: Topolight Effects in

Photonics” and it is scheduled for March 2015. Furthermore, the members of NL are invited to participate in the organizing committees of international conferences or workshops.

The research activities of NL are mainly supported by the local government (PAT), by the European Commission within the research frameworks, by the Italian Ministry of Education, University and Research (MIUR) and by companies. During the period covered by these Highlights, NL has been and is involved in the following projects: SiQuro (supported by PAT), projects on Mid-wave infrared super-continuum generation from silicon waveguides (supported by the CARIPLO foundation), collaborative project Italy-India (ITPAR) on green nanophotonics supported by MAE, FIRB NEMATIC: Nanoporous materials: self-assembled blackboard to study structure and interactions of DNA supported by MIUR, European projects within the 7th Framework: POSITIVE (FP7-ICT-257401), SYMPHONY (FP7-ICT-2013-10), IRIS” (FP7-ICT-2013-11).

Silicon Nanophotonics

Silicon photonics is the technology where photonic devices are produced by standard microelectronic processes using the same paradigm of electronics: integration of a large number of devices to yield a high circuit complexity which allows for high performances and low costs. Here, the real truth is to develop photonic devices that can be easily integrated to improve the single device performance and to allow high volume production.

We are involved in researching new optical scheme for implementing optical network on a chip by using concepts of nanophotonics. We use the concept of whispering gallery modes which develops in micro-disks or micro-rings to further tune the photon mode density. These disks or rings are coupled directly with narrow mode SOI (Silicon-on-Insulator) waveguides. High quality factor cavities allow studying fundamental quantum optics concept such as optical forces. Series of coupled micro-rings are studied to study chaos and resonant feedback among different rings.

To develop silicon photonics, one further add-on is making silicon do something which it is not able to do in its standard (bulk) form. Low dimensional silicon, where small silicon nanocrystals or nanoclusters (Si-nc) are developed, is one way to compel silicon to act as an active optical material. The key ingredient that makes Si-nc appealing for photonics are: quantum size effects which make new phenomena appear in silicon, such as room temperature visible photoluminescence, optical gain, coulomb blockade and multiexciton generation. Our research interests are to exploit quantum confinement and reduced dimensionality to produce effective light sources, nonlinear optical devices and optical amplifiers. In addition, we use strain engineering to break the crystalline symmetry of silicon and look for parametric down conversion effects.

Nonlinear optics is used to generate pairs of entangled photons which in turn feed quantum interferometers or integrated photonic circuits.

Nanobiotechnologies, antioxidants and human health

All the aspects related to the nano-bio interfaces (which

are the structures where the co-existence of physical principles and biological molecules is clearly evident) are a challenging field of research. Though the leading research concerns the design, synthesis and dynamic behavior of nano-structured bio-interfaces, more specifically we are working on three research topics: silicon- and based nanosystems, cellulose nanofibers, and antioxidant behavior in micelle systems.

To develop silicon based bio-sensors, we are currently focused on silicon based hybrid nanostructures. In particular silicon or silicon nitride flat or porous films are the starting inorganic support into which bio active layers are designed. Biological recognition elements are introduced on this hybrid layer. Molecular surface density, active layer thickness and integration of the bio-active interface with photonic devices will be the future challenges to develop the sensor system.

Beyond traditional analytical applications, silicon nanostructures can be used as “nanosensors” or “nanotools”, which permit to monitor the intracellular events or dynamically interact with the cellular environment without introducing irreversible perturbations. In fact silicon nanostructures have a high aspect ratio, a surface with tunable chemical and physical characteristics and an intrinsic photoluminescence emission. Finally, silicon is highly compatible with the biological environments. These peculiar properties permit the design of platforms aimed at the delivering of bioactive molecules or at the tracking of intracellular events. We have been studying the nanostructure synthesis and coating to increase and stabilize the photoluminescence emission and decrease toxicity. We demonstrated that nanostructured silicon microparticles we produce are efficiently and safely up-taken by human cells and do not show any toxic effect. Moreover conjugation to biological molecules and strategies to increase cell uptake and control intracellular localization are future steps of this research.

We have recently started a new research activity concerning the preparation of cellulose nanofibers (NCF) starting from wastes of wood industry. We are interested in the mechano-chemical properties of these nanostructures and in the synthesis of hybrid systems for sensor applications.

Antioxidant compounds are able to control reactive and damaging forms of oxygen, referred to as free radicals. Though antioxidants have been largely studied, much remains unknown about the human body adsorption and use of these compounds. We are investigating the synergistic effect of plasma antioxidants at the interface of micelle systems. Beyond the basic biophysical investigation, the crucial point is the development of devices and methodologies to monitor the antioxidant action. Being these processes free-radical mediated, a very high detection sensitivity is required. Moreover, to have physiological significance, the experiments should be performed in heterogeneous systems mimicking an un-perturbed biological environment. Thus we are proposing a new theoretically based methodology to compute antioxidant capacity and efficiency starting from oxygen concentration measurement, as well as, we are designing a nanostructured electrode to monitor molecular oxygen in real time.

Experimental facilities

The NL facilities allow for detailed experimental studies in nanoscience, photonics and biotechnologies. Since the effective collaboration with FBK most material processing and device productions are performed within their premises. For photonics, we have facilities to cover the light spectrum from the THz to UV ranges with whatever time resolution is needed. Laser sources comprehends: Ti:sapphire fs-ps laser (1 W average over 1000-700 nm, 2 ps or 70 fs pulses, 82 MHz repetition rate) interfaced with a second harmonic generator and pulse picker; Nd-Yag laser interfaced with an optical parametric oscillator which allows scanning the 400-3000 nm wavelength region (pulse 50 mJ, 10 ns, 10 Hz); TOPAS pumped with an amplified Ti:Sa laser which covers the 1-2.6 μm range with 35 fs, 10 kHz, 3 mJ; one CW, UV extended, Ar laser; three tunable CW lasers (850-870 nm, 1200 - 1700 nm and 1500 - 1600nm) fiber pig-tailed; high power fiber-laser at 1550 nm (1-100 MHz, 50 ps); 4W EDFA and 2W semiconductor amplifiers, several pig-tailed diode lasers, ASE source at 1550 nm and a broad band SLD at 800 nm. Three high-power true-CW DPSS single-line laser operating at 532 , 473 and 355 nm. Detectors comprehend: visible and infrared photomultipliers and CCDs, a streak camera with ps resolution, 4K cooled bolometers which cover THz region, avalanche photodiodes for vis and IR ranges plus one capable of photon-counting in the third telecom window. IR and MIR cameras. To perform spectral analysis several set-ups are available: FTIR and dispersive spectrophotometers, a micro-Raman setup, a micro-FTIR and a UV-vis-IR spectrophotometer (shared with other laboratories), UV-Vis and fluorescence spectrophotometer dedicated to biochemical experiments. Five dedicated apparatus for WG characterization equipped with nanopositioning systems and polarization controllers are available, each one specified on a given functions: visible, infrared, pump-probe, grating coupling and non-linear measurements. Other apparatus are: - visible and infrared photoconductivity set-up; - a solar simulator for cell sizes up to 5 inches; - two nano-probe stations (AFM and SNOM) - two semiconductor probe stations (4 and 8 inches) and many different electrical characterization set-ups (I-V, Z- ω , EL-I, etc.). Two VIS to NIR optical spectrum analyzers are available to NL-Lab. A probe station is fiber-bunch interfaced with a spectrometer interfaced with IR and visible liquid nitrogen cooled CCDs. For sample treatment and high sensitivity analytical detection, an electrochemical laboratory equipped with several chemical hots, spinners, galvanostates and voltammeters is available. An electron beam lithography set-up (SEM attachment) is also owned. For optical, electrical and molecular dynamic simulations, the laboratory uses free and commercial software, a dedicated cluster with 16 nodes and work-stations. Two laboratories, one dedicated to chemical synthesis and the second to biological sample preparation, are also available.

2014 Publications:

1. "Hybrid Materials for Integrated Photonics", P. Bettotti, *Advances in Optics* 891395 (2014).
2. "Electrical Conductivity of SiOCN Ceramics by the Powder-Solution-Composite Technique", Van Lam Nguyen, Caterina Zanella, Paolo Bettotti and Gian Domenico Sorarù, *J. Am. Cer. Soc.* 97, 2525 (2014).
3. "Role of nonspecific binding: a comparison among flow through and flow over assays in nanoporous material", P. Bettotti; N. Kumar; R. Guider; E. Froner; M. Scarpa, *Proc. SPIE* 8954, *Nanoscale Imaging, Sensing, and Actuation for Biomedical Applications XI*, 89540T (2014).
4. "Orange and blue luminescence emission to track functionalized porous silicon microparticles inside the cells of the human immune system." N. Daldosso, A. Ghafarinazari, P. Cortelletti, L. Marongiu, M. Donini, V. Paterlini, P. Bettotti, R. Guider, E. Froner, S. Dusi and M. Scarpa, *J. Mater Chem. B* 2, 6345 (2014).
5. "Reaction rates of α -tocopheroxyl radicals confined in micelles and in human plasma lipoproteins", P. Vanzani, A. Rigo, L. Zennaro, M. L. Di Paolo, M. Scarpa, M. Rossetto, *Biophysical Chemistry* 192, 20 (2014).
6. "Investigation of non-specific signals in nanoporous flow-through and flow-over based sensors" N. Kumar, E. Froner, R. Guider, M. Scarpa and P. Bettotti, *Analyst* 139(6), 1345 (2014).
7. "Self-detachment of free-standing porous silicon membranes in moderately doped n-type silicon", N. Kumar, S. Gennaro, V. S. Pradeep, G. D. Soraru, P. Bettotti, *Appl. Phys. A* 116, 251(2014).
8. "Evanescent-Field Excitation and Collection Approach for Waveguide Based Photonic Luminescent Biosensors", E. Rigo, F.J. Aparicio, M.R. Vanacharla, S. Larcheri, R. Guider, B. Han, G. Pucker, and L. Pavesi *Applied Physics B: Lasers and Optics* 114, 537-544 (2014).
9. "Chaotic dynamics in coupled resonator sequences", M. Mancinelli, M. Borghi, F. Ramiro-Manzano, J.M. Fedeli. L. Pavesi *Optics Express* 22, 14505 (2014)
10. "High Detection Efficiency and Time Resolution integrated-passive-quenched Single Photon Avalanche Diodes" F. Acerbi, M. Cazzanelli, A. Ferri, A. Gola, L. Pavesi, N. Zorzi, C. Piemonte *IEEE Journal of Selected Topics in Quantum Electronics* 20, 3804608 (2014).
11. "Characterization of Single Photon time resolution: from single SPAD to Silicon Photomultiplier" F. Acerbi, A. Ferri, A. Gola, M. Cazzanelli, L. Pavesi, N. Zorzi, C. Piemonte, *IEEE Transactions on Nuclear Science* 61, 2678 (2014).
12. "Silicon Oxynitride Waveguides as Evanescent Field Based Luminescent Biosensors" Aparicio Rebollo, Francisco Javier; Froner, Elena; Rigo, Eveline; Gandolfi, Davide; Scarpa, Marina; Han, Bing; Ghulinyan, Mher; Pucker, Georg; Pavesi, Lorenzo *Journal of Physics D: Applied Physics* 47, 405401 (2014).
13. "Inter-mode reactive coupling induced by waveguide-resonator interaction" Mher Ghulinyan, Fernando Ramiro Manzano, Nikola Prtljaga, Martino Bernard, Lorenzo Pavesi, Georg Pucker, Iacopo Carusotto *Physical Review A* 90, 053811 (2014).
14. "Nonlinear self-polarization flipping in silicon sub-wavelength waveguides: distortion, loss, dispersion

and noise effects” Wen Qi Zhang, M. A. Lohe, Tanya M. Monro, Paolo Bettotti, Lorenzo Pavesi and Shahraam Afshar V *Optics Express - Nonlinear Photonics Focus Issue*, 22, 27643 (2014).

15. “Silicon based optical resonators” A. Pitanti, P. Bettotti, M. Ghulinyan, L. Pavesi in *Nanostructured Semiconductors: from basic research to applications*, edited by P. Granitzer and K. Rumpf (Pan Stanford Publishing Ltd, Singapore 2014) chapter 12

2014 Books-special issues:

1. *Light Localisation and Lasing: Random and Pseudorandom Photonic Structures*, Mher Ghulinyan and Lorenzo Pavesi, Cambridge University Press (2014)
2. *Silicon Photonics and Photonic Integrated Circuits IV* Laurent Vivien, Seppo K. Honkanen, Lorenzo Pavesi, Stefano Pelli, Proceedings of the SPIE, Volume 9133 May 2014
3. *Silicon Photonics*, guest editors Vivien, Laurent; Cheben, Pavel; Lo Guo-Qiang, Patrick; Pavesi Lorenzo, IEEE Journal of Selected Topics in Quantum Electronics, 20(4) (July/August 2014)

1. Truly random number generation exploiting silicon nanocrystal LEDs (Zahra Bisadi)

Generation of truly random numbers is absolutely necessary in many applications such as Monte Carlo simulations and particularly cryptography where producing unpredictable results is vital to guarantee complete security of data transmission. In several situations, random numbers are obtained through pseudo random number generators (PRNG) which are deterministic algorithms able to output long sequences of bits at high bit-rates. However, their unpredictability is not totally assured since when the seed (initial value) is revealed, all the bits in the sequence will consequently be constructed. Contrary to pseudo random numbers, truly random numbers essentially need to be generated through physical non-deterministic processes.

Inherent randomness and indeterminacy provided by quantum physics can be exploited advantageously to generate random numbers. Quantum dots, single photon avalanche photodiode (SPAD), light emitting devices (LEDs), and laser have been employed as sources of entropy to produce random numbers.

Taking into account the non-deterministic process of spontaneous emission of photons in silicon nanocrystal (Si-NC) LEDs, we employed them to generate quantum random numbers. The light emitted from the LED was transmitted through a bundle of optical fibers to a SPAD and then a multichannel scaler (MCS) connected to a PC through which sequences of bits were extracted fixing a bin-width of $1\mu\text{s}$. To evaluate the randomness of the bit sequences, we made use of the statistical tests in NIST test suit. The generated bit sequences passed all the NIST tests except one, the Runs test. By enforcing a dead time of length equal to the bin-width and half the bin-width, the datasets passed all the NIST tests (the analysis was done using 100 sequences of 106 bits). Data extraction process can be seen schematically in Figure 1 below.

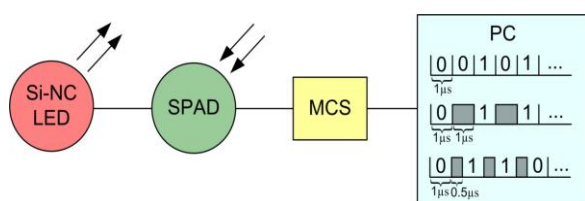


Figure 1. Schematic of the experimental setup and bit sequence extraction

The quantum random number generator (QRNG) we produced enjoys the two main advantages of very negligible bias and simple setup with a bit-rate of 0.6Mbps which is relatively low compared to existing physical RNGs. However, our approach benefits from utilizing light to stimulate events in the SPAD and it avoids a deterministic post-processing of the raw data. This fact is extremely remarkable in producing high quality random numbers and compensates for the low bit-rate. The overall bit-rate can be easily increased by adopting a parallel architecture and exploiting the CMOS compatibility of all components.

2. Microrings and Mach Zehnder based biosensors for Aflatoxin detection in milk (Davide Gandolfi, Tatevik Chalyan, Romain Guider)

Since November 2013, the Nanoscience Laboratory is involved in the European Project SYMPHONY. The objective of this project is the creation of a novel analytical platform to detect Aflatoxin in milk and prevent infection of dairy products. In order to achieve such a goal, our group will design and test a photonic sensing device based on photonic resonators integrated in microsystem technologies, for highly sensitive detection. With the use this technology, we aim to achieve the characterization of miniaturized smart system that will perform low cost label free detection.

During the first year of this project, we designed, developed and tested two types of photonic sensors in order to define their performances in term of Aflatoxin sensing. The first design is based on SiN asymmetric Mach-Zehnder Interferometers (aMZI) and it has been developed by LioniX. The second sensor is based on SiON microring resonators (mRR) and it has been developed jointly by FBK and UniTN.

Innovative designs were simulated and tested. In addition, we established close collaborations with the other partner teams for the development of a reliable functionalization procedure as well as a smart and compact microfluidic platform.



Figure 2. Picture of an optical sensor chip in the microfluidic system. In both cases, we were able to measure high sensitivity and obtained LOD of 0.8×10^{-6} RIU and 1.6×10^{-6} RIU in the case of aMZI and mRR, respectively. Preliminary Aflatoxin sensing measurements are also available.

3. Mechanical stress in porous silicon free standing membranes (Paolo Bettotti, Cristina Traversa, Romain Guider)

Porous silicon free standing membrane is a unique material with great potential in applied physics [1]. The largely tunability of the porous structure permits to fabricate membranes with a wide range of optical and mechanical properties. One of the main limits of free standing membranes is their low mechanical robustness: thin layer are difficult to handle because of their intrinsic fragility, but thick membranes tend to roll up forming macroscopic cracks.

In the last year, we have demonstrated that porous silicon layer accumulates a compressive stress during the etching process, which is partially compensated by the presence of the substrate. In the case of FSMs, this stress is released as demonstrated by the macroscopic bending of the mem-

branes. To prove it, we did Raman analysis on both free standing and supported porous silicon layers and observed that the substrate partially compensates the stress accumulated by the porous layer during the etching. As the values extracted from Raman peaks measured on PSL are averaged by the compressive stress of the porous layer and the compensating effect of the substrate, the analysis of FSM are essential for studying stress in porous materials. Moreover, we demonstrated that the size distributions of the PSi skeleton on concave and convex surfaces of the free standing membrane are different and, in particular, the convex surface has a broader size distribution of silicon nanostructures. This fact is compatible with a reminiscence of the larger concentration of Si nanocrystals created during the chemical etching.

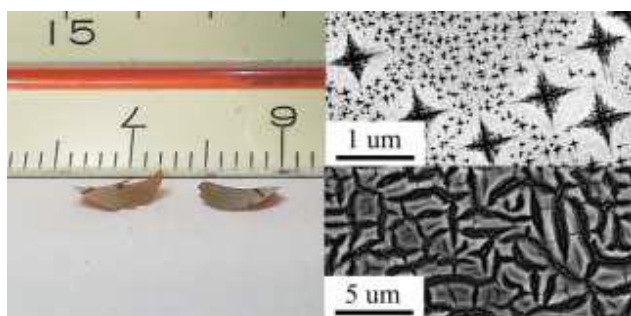


Figure 3. (a) Photograph of released FSMs which are bent by the mechanical stress accumulated during their etching. (b) Defects on the porous silicon surface: (top) larger pores decorate the surface of surface of a free standing PSi membrane etched in n^+ Silicon. The anisotropy of the etching is clearly underlined by the star shaped pores which indicate the $\{110\}$ lattice directions (scale bar $1 \mu\text{m}$). (bottom) Top surface of a p^+ sample. The dark grooves are the result of the collapsing of neighbor pore walls (scale bar $5 \mu\text{m}$).

The results from this study give a clear description of the Raman properties of silicon nanostructures and can serve as a starting point to fabricate samples with optimized mechanical properties.

References

1. N. Kumar, E. Froner, R. Guider, M. Scarpa and P. Bettotti, "Investigation of non-specific signals in nanoporous flowthrough and flow-over based sensors," *Analyst* 139(6), 1345 (2014)

4. Multiple wavelengths coupling in vertically coupled wedge resonators (Fabio Turri)

WGM resonators are becoming fundamental building blocks for the modulation and manipulation of optical signals in integrated devices. For an efficient application of these elements integration of both the resonator and the coupling element is of crucial importance; in this sense a promising coupling technique is that of vertical coupling

where the coupling waveguide lays under the resonator edge (Figure 4).

We demonstrated coupling of light into a vertically coupled wedge Whispering Gallery Mode (WGM) resonator over a wide wavelength range (from 760 to 1630). This property is due to the widespread coupling region that arises when vertically coupled structures are considered: the coupling mechanism becomes very similar to the one found in a common directional coupler (see Figure 4). It is important to notice that this unique feature is not observed in the in-plane coupling configuration.

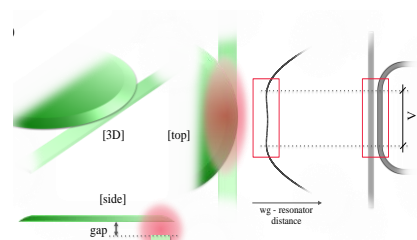


Figure 4. On the left side a schematic representation of the vertically coupled wedge resonator is shown, with the coupling region evidenced in red; on the right side wg-resonator effective distance is compared to a directional coupler to evidence the similarity between the two.

In Figure 5 experimental data are shown and coupling of light in the IR and the visible range is clearly observed. Oscillations in the transmittance dip are also observed and they resemble the behaviour found for directional couplers and explained by Coupled Mode Theory. On the basis of a previous work, an analytical model for the vertical coupling geometry has been extended and compared to experimental data in the IR range. Good agreement between the two has been found (Figure 5 - pink line).

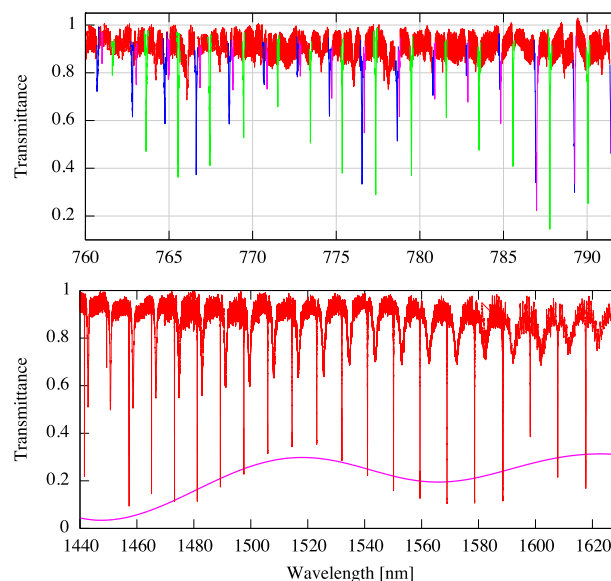


Figure 5 Visible spectrum is shown on the top with different radial family modes evidenced using different colours: coupling periodic oscillation of the transmittance dip is clearly observed.

The possibility to couple over a large wavelength range (more than 500nm) represents a great improvement in integrated photonics since it allows multiple channel data elaboration to be performed on a single device, thus increasing the # of operation / device.

5. Time resolved micro-fluorescence detection of electrophoresis systems (Sanjay B. Thorat, Paolo Bettotti)

Capillary electrophoresis (CE) is an important analytical tool used for separating chemical species on the basis of charge-to-size ratios. In the analytical sciences it has been used for separation and purification of chemical species. There are different types of detection systems used in CE, such as absorption, fluorescence, electrochemical and refractive index based. Amongst these methods, laser-induced fluorescence (LIF) detection is the most sensitive, capable for single molecule detection and requires small volume.

LIF detection based electrophoresis is a completely new research activity in our research group and also keeping in mind the use of such system in the NEMATIC project. So it is important to assemble such setup in-house for further research activity. In this regards, we have successfully developed LIF-based detection for electrophoresis system. In particular, we have used silica nanoparticles (20 nm) functionalized with silane followed by fluorescein isothiocyanate (FITC) dye. The glass micropipettes were used for CE experiments. The capillary was filled with functionalized silica and copper wire was placed from both end of the capillary. The system was connected to DC power supply to introduce electric current into system. The whole micro-capillary setup was placed on glass slide and then fixed on the inverted microscope. The laser (488 nm) was incorporated in to the inverted microscope setup. Moreover, high precision camera was placed on microscope to visualize the movement of NPs inside the capillary. By applying the voltage and inducing laser to the system, we have visualized the movement of silica nanoparticles inside the capillary and these observations were complimented with time-resolved fluorescence spectra. Furthermore, we have studied the effect of polarity change. The direction of movement of NPs changes, when the polarity changes along the capillary. Similarly, we observed the peak intensity change in fluorescence spectra as polarity changes. Additionally, the lower detection limit for the LIF based system was found by diluting the mother liquid of FITC (26.38 μM) with ultrapure water down to 33 pM concentration. In Fig.1. A photoluminescence spectrum (PL) for 0.33 nM FITC solution is shown.

In conclusion, we have developed a LIF based setup for CE and visualized the movement of NPs inside the glass micro-capillary. Also the lower detection limit of our system was investigated and will be beneficial for future project of DNA analysis and separation.

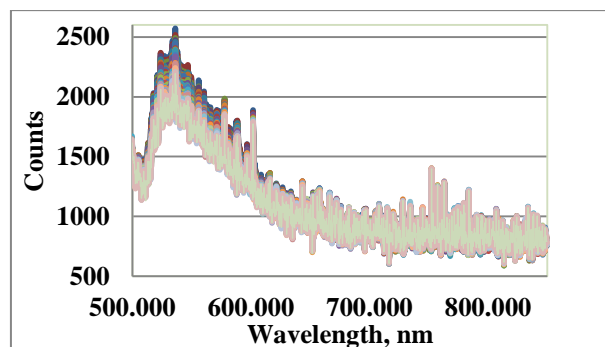


Figure 6 Detection limit: PL spectra for 0.33 nM FITC solution

6. Novel design of Array Waveguide Gratings for a Silicon Photonics based Optical Network (Stefano Tondini, Mattia Mancinelli)

Starting from January 2014, the NanoLab is involved in the IRIS, a European Project that aims at fabricating an highly integrated WDM photonic switch to be inserted as transponder aggregator into the existing optical transport network. The target is the realization of a silicon photonics based sub-system for Metro application driving 48 optical channels, with 100 GHz spacing in the C-band, 4 different directions and 12 add/drop channels. The provided flexibility, energy efficiency, small footprint and fast reconfigurability (microsecond regime) will definitely lead to a paradigm change in the deployment of optical communication, without disrupting the current ROADM architecture.

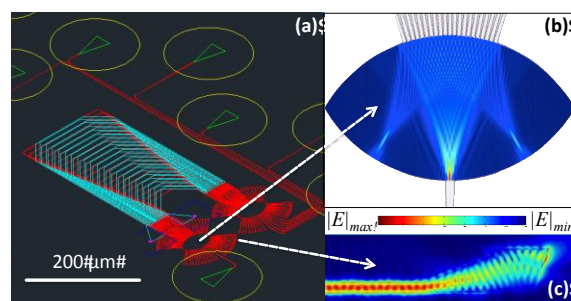


Figure 7. (a) One of the array waveguide grating designs that have been proposed in order to match the IRIS requirements: in red the silicon waveguides, the light blue strips represent the heating circuit to be placed on the top of the array, the dark background is the SiO₂ substrate and the green tangles are grating couplers to inject or collect the signal through the device. Special effort was applied in minimizing crosstalk and in optimizing the design of the star coupler regions. **(b)** Stationary solution obtained for the star coupler region when the input channel is on. **(c)** Asymmetric tapering design, which leads to an improved suppression of the back-reflected light within the free propagation regions

Within this frame, the NanoLab is asked to develop and validate an high-resolution AWG design able to match unprecedented requirements: insertion loss < 3dB, X-talk < -20dB and scaled footprint.

In order to improve the performances and keep down the footprint, a set of procedures leading to a novel design for silicon-on-insulator (SOI) AWGs has been proposed [Figure 7 (a)]. Parameters such as waveguide width, tapering length, bending radius and star-coupler shape have been extensively searched through FEM simulations [Figure 7 (b) and (c)]. Using COMSOL Multiphysics we computed effective indices as well as mode profiles of each building block at a wavelength of 1.552 μm . Then we performed a complete sweep for values between 1.540 and 1.565 μm , in order to test the components within the operation range. Special attention was paid to the free propagation of beams at the star couplers, which has been simulated analytically in the Fraunhofer approximation. By means of MATLAB we estimated the electric field overlap at each interface/connection, ultimately choosing the best dimensions for the design in terms of insertion losses and X-talk. Heating circuits have been also designed in order to apply on each waveguide the same phase shift causing an overall tuning of the channel-output.

7. Role of the inversion layer in silicon nanocrystal based LEDs

By means of two Si-NCs based LEDs (W1 and W2), which are similar for active material but different in the fabrication process, we have been able to elucidate the role of the non-radiative recombination rates at the active layer/substrate interface.

The devices structure is a MOS capacitor (Figure 8 (a)) where alternating stoichiometric SiO₂ and Si-NCs (annealed silicon-rich-oxide) layers, repeated in sequence, are used as gate oxide. These multilayers (ML) were fabricated via PECVD on 4 inch p-type silicon substrates and subsequently thermal annealed.

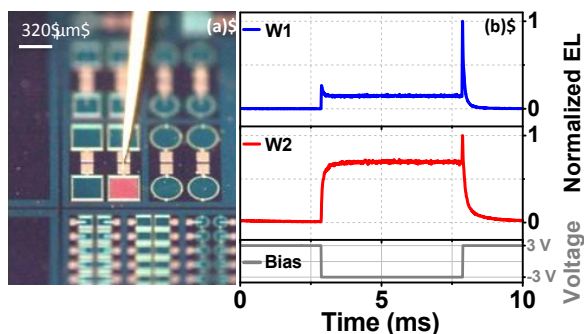


Figure 8. (a) Picture of W2 sample when biased @ -5V. The typical red emission of Si-NCs is clearly visible. (b) Comparison between time-resolved EL signal collected for W1 and W2 respectively. Below the two plots is reported the pumping scheme used to drive the devices

I-V sweeps show a non-rectifying behaviour for W1, while a marked rectifying behaviour is shared by W2. The reason lies at the interface between the substrate and silicon-rich-oxide ML stack, where under reverse bias an external inversion layer with a fast rate of minority carrier generation forms for W1 but not for W2. This is demonstrated by performing C-V sweeps.

By comparing the fabrication processes of the two LEDs a significant difference is found in the thermal treatment, which have caused a different quality of the oxide, which, in one case, is well insulating and, in the second, leaks through. This fabrication difference leads to a MOS-like behaviour of W1 and to a p-i-n-like behaviour of W2. Time-resolved EL measurements (Figure 8 (b)) yield more direct information on the carrier dynamics during device operation. Using a square waveform as bias there is the possibility of sequentially injecting opposite carriers into the Si-NCs material, which subsequently recombine radiatively. This is pointed out by the presence of EL overshoots when the supply voltage is swept abruptly from positive-to-negative value and vice versa. EL spikes are associated with the increased probability of radiative recombination of the excitons, which remain inside the Si-NCs when the voltage is abruptly switched. W1 shares this behaviour. On the contrary, W2 (rectifying I-V characteristic) presents a lower EL emission peak only during forward-to-reverse bias transitions. In fact, since in W2 no inversion layer takes place, no electrons can be injected under reverse bias from the substrate through the ML. Consequently no trapped carriers are released to originate the EL overshoot at the reverse-to-forward bias transition.

8. A set-up for the generation of entangled photons via second order parametric processes (Alessandro Trenti)

The study of quantum states of light is a rapidly developing field of research. In recent years, scientists have begun to find situations where quantum mechanically systems provide unique solutions to modern technological problems. Quantum information processing (QIP) is an exciting example of promising applications of such systems. This is the framework of the SIQURO project.

SIQURO aims at bringing the quantum world into integrated photonics by using the silicon platform and, therefore, permitting in a natural way the integration of quantum photonics with electronics. In this way, by using the same successful paradigm of microelectronics, the vision is to have low cost and mass manufacturable integrated quantum photonic circuits for a variety of different applications in quantum computing, secure communications and services. This will be achieved on one side by engineering the optical properties of silicon by using nanotechnology and material sciences and on the other side by developing suitable quantum theories to predict the properties of photons in such a specific systems.

An experimental set up has been mounted able to generate IR twin photon pairs by Spontaneous Parametric Down Conversion (SPDC) in a periodically poled Magnesium doped Lithium Niobate (PPLN MgO:LiNbO₃) crystal using a 775 nm pump Titanium Sapphire continuous wave laser. Photon pairs created by Spontaneous Parametric Down Conversion (SPDC) are one of the most stable, high brightness and promising sources of quantum light. SPDC, which in the old literature was frequently referred to as parametric fluorescence or parametric scattering, is a second-order nonlinear optical process in which a high fre-

frequency photon spontaneously splits into two lower frequency photons. It is thereby the inverse process of the more widely known up conversion processes of second-harmonic generation (SHG) and sum frequency generation (SFG), where two low frequency beams are nonlinearly mixed to produce one high frequency component. Experimentally after having verified the occurrence of SPDC, we proceeded to assess the correlated properties of the photon pairs. One approach is to perform a coincidence measurement, as sketched in Figure 9.

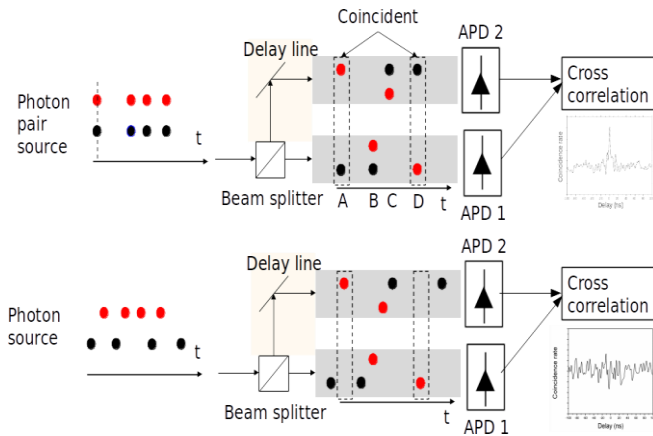


Figure 9. Sketch of the coincidence set-up. On the left is reported a schematic representation of a standard photon source and of a time-correlated photon source. (A,B,C,D) All the possible paths of a photon pair.

The time correlated nature of the generated photons can be demonstrated by exploiting the fact that the photons are randomly generated in pairs and at the same time. As shown in Figure 9 this approach requires the use of a balanced beam splitter, in our case directly integrated in fiber. Only a photon pair can generate an avalanche at the same time in both the APDs giving rise to a coincidence event. The expected rate of coincidences is of the same order of magnitude as the measured values of the peaks that stand out on the background of accidental coincidences. Moreover the fact that the cross correlation curve in the case of a classical photon source does not show any peaks ensures that the peak found in the case of SPDC photon source is due to time correlated photon pairs.

9. Multi-mode interference revealed by two photon absorption in silicon rich SiO₂ waveguides (Santanu Manna, Fernando Ramiro Manzano)

Non-linear silicon photonics is a rapidly emerging field drawing significant attention due to the possibility of all optical signal processing employing the existing mature planar Si technology. Owing to the significant optical nonlinearities, Si NCs can be chosen as active material in non-linear photonic devices. Several papers have reported a larger third order non-linearity for Si NCs than for bulk silicon, because of both quantum confinement and dielec-

tric mismatch phenomena. Though the nonlinear losses due to the two-photon absorption (TPA), excited free carrier absorption and defect-induced absorption are often considered to be limiting factors, they can be also employed to enable certain functional devices. In our work, we have proposed a method to use TPA induced photoluminescence (PL) to map the spatial multimode interference profile of a Si NC waveguide. The proposed method can be used for other material systems provided that luminescence can be excited by TPA. In terms of basic research, it should help in the future to create or improve computer models that should reproduce the real interference with/without scattering centers.

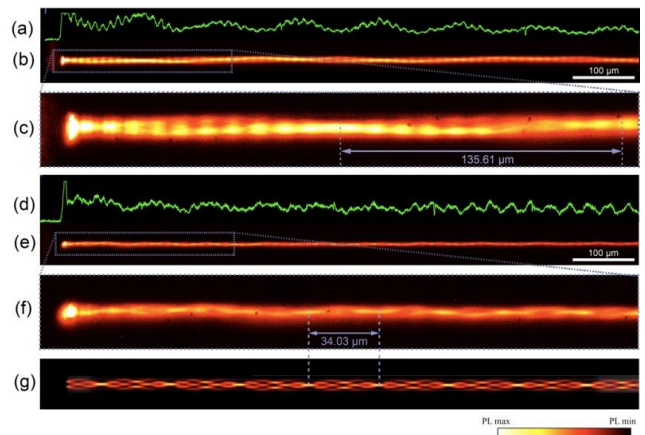


Figure 10. (a) Integrated intensity profile of the TPA excited PL as a function of the position when a line scan through the center of the waveguide is performed. Data refer to the 10 μm wide sintered waveguide. (b) TPA excited PL image of the waveguide. (c) Same as (b) but with an increased magnification. The bar refers to the beat length. (d) Integrated intensity profile of the TPA excited PL as a function of the position when a line scan through the center of the waveguide is performed. Data refer to the 5 μm wide sintered waveguide (e) TPA excited PL image of the waveguide. (f) Same as (e) but with an increased magnification. The bar refers to the beat length. (g) COMSOL simulation for the 5 μm waveguide.

Firstly, to characterize non-linear TPA, β (TPA coefficient) has been estimated utilizing the transmittance measurement through the Silicon Rich Oxide (SRO) waveguides pumped by a 1550 nm pico-second laser. The behavior of the transmitted power with the variation of input power changes from linearity to non-linear one due to the additional quadratic power loss through TPA. Calculated values of β corresponding to 1550 nm wavelength are of the order 10^{-8} – 10^{-9} cm/W, which is more than one order compared to the bulk silicon. We have noticed a change in β as the Si content varies, indicating that the band detuning is responsible for efficient two photon absorptions. When the Si NC waveguides are pumped by a 1550 nm pico-second laser, two photon absorption excites electrons in Si-NC. The excited electron relaxes quickly to the minima of the excited state band and decays to the ground state either by photon emission or by a non-radiative process.

This TPA assisted PL emission was collected from the top of the Si NC waveguides.

Figures 10 (a–c) shows the information for the 10 μm wide multimode G10 sintered waveguide. Visible image of the TPA induced PL emission from this waveguide shows that the intensity decreases with the distance due to the signal depletion caused by the nonlinear absorption along with clear oscillations in the TPA assisted PL signal. These oscillations are due to the interference of the propagating 1550 nm optical modes in our multimode waveguide. TPA tracks this multimode interference pattern and so also the TPA excited PL intensity. Figures 10 (d–f) report the same information for the 5 μm wide multimode sintered waveguide. A comparison with the multi-mode interference pattern simulated using COMSOL for this specific waveguide is shown in Fig. 10 (g). The agreement between the measured mode profile and the simulated one is remarkable. The experimental beat note data have been extracted by performing Fast Fourier Transforms of the spatial profiles of the TPA-PL emission through the centre of the waveguides. For the 5 μm and 10 μm waveguides, the beat lengths of multimode interface (MMI) pattern have been found to be 34.03 μm and 135.61 μm , respectively, agreeing well with the theoretical beat lengths ($L_\pi = \pi / (\beta_0 - \beta_1)$), where $\beta_{1,2}$ are the mode propagation constants of the two lowest order modes in a multimode waveguide). Shortening of the beat length in the narrower waveguide follows self-imaging effect characteristics of multimode interference.

As a conclusion, we have reported that the observation of the fluorescence light (induced by two photon absorption) is a very interesting tool to map the intensity profiles of the 1550 nm propagating optical modes in multimode waveguides.

10. Intermode reactive coupling induced by waveguide-resonator interaction (Fernando Ramiro-Manzano)

The study of the consequences of coupling a physical system to an environment constitutes the central problem in the theory of open systems. This coupling, on one hand, allows the system to dissipate energy through active decay channels. On the other hand, its reactive component leads to a shift of energy levels and oscillation frequencies of the system. Most celebrated examples of this physics involve an atom coupled to the bath of electromagnetic modes, namely, the (dissipative) spontaneous emission of photons from an excited state and the (reactive) Lamb shift of transition frequencies.

In photonics, the presence of a waveguide in the vicinity of a resonator activates new radiative decay channels for the resonator modes via emission of light into the waveguide mode. The corresponding reactive effect is a shift of the resonator mode frequencies, which can be interpreted as the photonic analogue of the atomic Lamb shift. We reported on a joint theoretical and experimental study of a photonic device in which pairs of modes of very similar frequencies are coupled simultaneously to the same waveguide mode. Both the dissipative and the reactive cou-

plings of the cavity modes to the waveguide turn out to be affected by interference phenomena between the two modes, which can be summarized as environment-induced intermode couplings: in the atomic analogy, the dissipative component gives a coherent population trapping phenomenon, while the reactive one produces a sort of *off-diagonal Lamb shift*. Our results show that the consideration of both of these coupling terms is necessary in order to explain the peculiar Fano interference line shapes experimentally observed in the transmission spectra of single resonators.

In the experiments, we looked at pairs of quasideviant modes originating from different radial families in micro-disk resonators coupled vertically to dielectric waveguides. The generality of our observations has been confirmed by experiments on a $R = 50 \mu\text{m}$ resonator in which the Fano interference takes place between the first and the third radial mode family, RMFs. The measured transmission spectra are shown in Figs. 11(a) and 11(c) for different values of the relative detuning of the quasideviant pairs of modes. The crossing of the two families again leads to Fano interference profiles, and the narrow feature disappears in a specific range of detunings (spectrum S9). Furthermore, the experimental results successfully compare to the prediction of the analytical model, generalized to three modes [Fig. 11(b)].

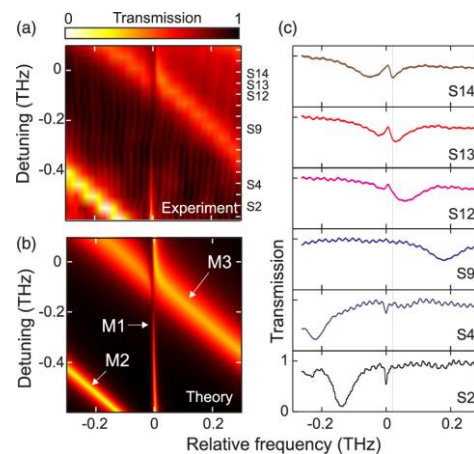


Figure 11. (a) Color map merging 21 experimental transmission spectra (indicated as S1–S21) for a 50 μm resonator. (b) Analytic prediction. (c) Selected examples of spectra.

References

1. M. Ghulinyan, F. Ramiro-Manzano, N. Prtljaga, M. Bernard, L. Pavesi, G. Pucker, I. Carusotto, Phys. Rev. A **90**, 053811 (2014)

11. Enhancement of photoluminescence intensity of erbium doped silica containing Ge nanocrystals: distance dependent interactions (Santanu Manna)

Modern fiber-optics communication system uses near infrared light at 1.54 μm wavelength, which coincides with minimum transmission loss of silica fibers. Erbium, is useful for optical signal amplification in fibers because of its $\sim 1.54 \mu\text{m}$ emission owing to the intra- $4f$ transition from

the first excited to the ground state (${}^4I_{13/2} \rightarrow {}^4I_{15/2}$). Since Ge, the other important Group IV element, has larger excitonic Bohr radius (~ 26 nm) compared to Si (~ 5 nm) leading to stronger quantum confinement, it might be a potential alternative material as a sensitizer for Er^{3+} ions. Additionally, the tunability of size dependent emission from sol-gel derived Ge NCs, and the possible improvement of the pumping efficiency due to the close value of the Ge exciton energy with the $1.54 \mu\text{m}$ transition from Er^{3+} ions motivate the use of Ge NCs as sensitizers for Er^{3+} ions.

Er-doped silica glass matrix containing Ge nanocrystals prepared by sol-gel method are described in this study. Different sets of sol-gel glasses have been prepared with varying Ge and Er fractions annealed at different temperatures. Ge nanocrystals of average diameter ranging from 4.1 to 6.8 nm show a broad photoluminescence (PL) peak being sequentially red shifted from 937 nm to 1038 nm in the near infrared region, as a function of size. Enhancement of $1.54 \mu\text{m}$ PL intensity is observed with increase in Ge content and annealing temperature of the glass composites. Time resolved measurements indicate that the decay time is as high as ~ 9 ms, which is reported for the first time for Ge nanocrystals based system. It has been shown that in presence of Ge NCs, the effective excitation cross section of Er^{3+} ion is enhanced by almost four orders of magnitude from $\sim 10^{-21} \text{ cm}^2$ to $\sim 10^{-17} \text{ cm}^2$. Our measurements also show that maximum 1.23% of total Er^{3+} ions could be indirectly excited by Ge NCs at a high pumping photon flux of $1.6 \times 10^{21} \text{ cm}^{-2} \text{ s}^{-1}$ (figure 12(a)). This is ascribed to the energy transfer from Ge NCs to Er^{3+} ions (schematically shown in figure 12(b)).

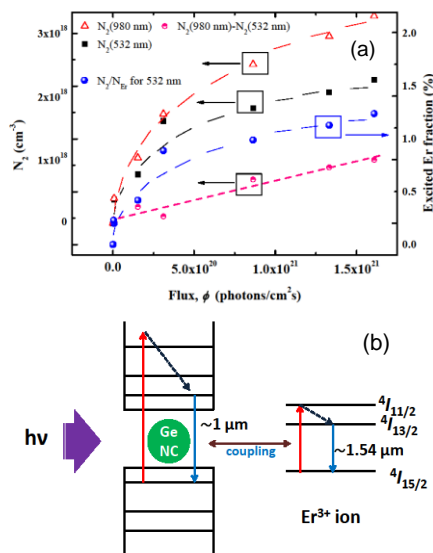


Figure 12. (a) Excited Er^{3+} ions density (N_2) as a function of the 980 nm (both direct + indirect excitation) and 532 nm (only indirect excitation) photon flux for 10% Ge, 1.5% Er annealed (850 oC) sample. The difference provides only directly excited Er^{3+} ions density. Indirectly excited fraction of Er^{3+} ions as a function of the 532 nm photon flux is also shown. All the dashed lines are guide to the eye. (b) Schematic diagram showing the coupling between a Ge NC and an Er^{3+} ion.

We modelled the Ge NC–Er interaction as a Dexter interaction which occurs with a characteristic interaction distance of ~ 0.2 nm. Dexter type energy transfer was confirmed from the exponential dependence of the effective excitation cross section of Er with the inter-distance between a Ge NC and Er ion. We also quantified the characteristic parameters for de-excitation phenomenon like cooperative up-conversion. However, the integrated Er PL intensity being temperature independent, corresponding to the sample of maximum excitable fraction, shows the huge suppression of non-radiative trap states. As a whole this work gives a range of parameters suitable to model the Er-Ge NC systems in order to optimize the material for all optical amplifiers.

References

1. S. Manna, R. Aluguri, R. Bar, S. Das, N. Prtljaga, L. Pavesi, and S. K. Ray, “Enhancement of photoluminescence intensity of erbium doped silica containing Ge nanocrystals: distance dependent interactions”, *Nanotechnology* **26**, 045202 (2015).

12. Selective mode coupling in multimodal silicon waveguides (Massimo Borghi and Mattia Mancinelli)

The different modes of waveguide propagate independently without power exchange. This feature can be exploited to multiplex signals at the same wavelength without channel crosstalk. In conjunction with Wavelength Division Multiplexing, Mode Division Multiplexing (MDM) further increases the aggregate bitrate of an optical channel.

The fundamental requirement for MDM is the ability to selectively excite only specific modes. In an integrated network, this is usually accomplished with the use of asymmetrical directional couplers or with Bragg gratings. The conversion efficiency between the incoming radiation and the excited mode is determined by wavevector conservation. In a directional coupler, the effective index of the input waveguide must match the one of the target waveguide. In a grating coupler, the periodicity of the grating allows wavevector conservation to be satisfied to less than a reciprocal lattice vector.

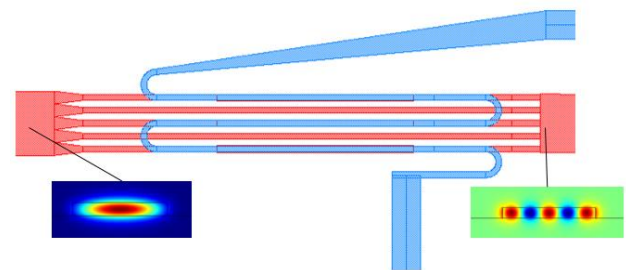


Figure 13. Schematic of first selective mode coupler. Light is input on the left side waveguide (red) and the target mode order is coupled on the right side. A metallic heater (blue) is placed on half of the branches to provide an additional π phase shift with respect to the other branches.

Within this context, we are developing two new coupling techniques for selective mode excitation. These methods

are based on the maximization between the overlap of the input electric field and the mode profile of the target waveguide. In this sense, they are fundamentally different from the ones based on phase matching. Figure 13 shows the first scheme. Light is butt coupled to the input waveguide with a symmetric field profile, as the one coming out of a standard single mode (SM) fiber. Light is then equally split into N, SM branches. Half of the branches provide an additional phase of π with respect to the others, thus creating the multi-lobe field pattern of the Nth mode of the target waveguide. The size and the spacing of the branches are optimized to maximize the overlap with the Nth mode profile.

In the second scheme, shown in Figure 14, we use the interference pattern created by two waves that travel with an angle θ with respect to each other to match the field profile of the Nth mode order.

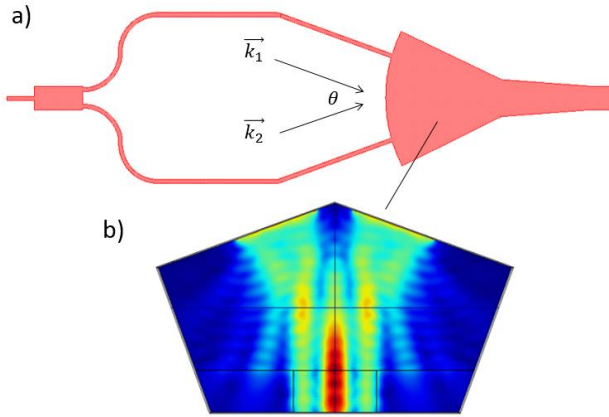


Figure 14. a) Schematic of second selective mode coupler. Light is input on the left side waveguide (red) and the target mode order is coupled on the right side. b) Finite Element Method simulation of the free space propagation region, showing the coupling of the third order mode to the waveguide (bottom).

Light is first butt coupled to the input waveguide, and a 3dB Multi Mode Interference device equally splits the signal into two SM waveguides. The latter end into a free space region forming an angle θ . The standing wave pattern has lobes which are 180° out of phase and separated by:

$$\Delta = \frac{\lambda}{n_{eff} \sin\left(\frac{\theta}{2}\right)}$$

By changing the angle we can match the lobe separation of the target multimode waveguide.

The mode overlap technique has the advantage to be more robust to fabrication defects with respect to phase matching based devices. On the other hand, the conversion efficiency is lower, with losses that could be as high as -2.5 dB.

13. Investigation of strain induced second order non-linearities in silicon through the Pockels effect in racetrack resonators (Mattia Mancinelli, Massimo Borghi)

The lack of χ^2 non-linearity in silicon has prevented SOI photonics to become a ‘complete’ platform for telecom applications because of the absence of electro-optic modulators and frequency converter. Recently, it has been shown that by breaking the silicon inversion symmetry, with the help of a stressing layer, it is possible to get a considerable effective χ^2 . Up to now, only 2 of all the χ^2 components of the strained silicon platform have been studied. Moreover, no model that links strain distribution to the resulting χ^2 tensor exists. This has prevented engineering of the material, for example, to maximize a particular χ^2 element.

The goal of our work is to map the complete tensor of the strained silicon platform and to develop a model to predict the χ^2 for any strain configuration with the help of a FEM software. The easiest way to access the χ^2 components is through the Pockels effect. Such effect describes how the waveguide's effective index (refractive index in a bulk) is modified by the interaction between the optical field and a DC field provided by metal contacts located close to the waveguide (see Fig. 15).

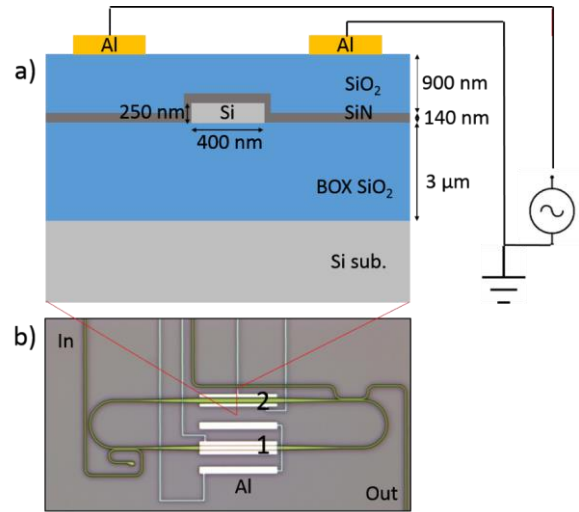


Figure 15. a) Device cross section whose top view is in panel b (red lines). b) Device top view. RTR with metal pads for two different DC field orientations: 1) vertical and 2) horizontal

An easy way to detect the effective index variation is to monitor the resonance position of a racetrack resonator (RTR). In this case, the effective index variation is linked to the χ^2 by the following relations:

$$\Delta n_{eff} = \frac{n_g}{2} E_k^{DC} \chi_{ijk}^{2\,eff} \chi_{ijk}^{2\,eff} = \frac{\int_{WG} \chi_{ijk}^2(x, y) E_i(\omega) E_j^*(\omega) dA}{\int_{\infty} n^2(x, y) E_i(\omega) E_j^*(\omega) dA}$$

where E^{DC} is the static field, n_g is the waveguide's group index and $\chi_{ijk}^{2\text{eff}}$ is the effective non-linearity that depends on the waveguide geometry. In our system, the two optical fields, $E_{i-j}(\omega)$, inside of the integrals are the same, $i = j$, thus they represent the modulus square of the optical field in the waveguide.

Figure 15 reports the system under study. Panel b) shows an optical image of the RTR (green) with a footprint of $190 \times 40 \mu\text{m}$ together with metal pads (white) to provide the DC field in both vertical (1) and horizontal (2) directions. Panel a) reports RTR cross-section in which all layers are visible: silicon WG (grey), silicon nitride stressing layer (dark grey), silica (blu) and Al metal pads (gold).

In order to access to different χ^2 components we designed RTRs (and thus waveguides) that are arranged at several angles, 0° - 30° - 45° - 60° - 90° , from the 111 crystallographic axis. Changing the angle changes the χ^2 element involved in the Pockel effect. Moreover, we included also RTRs with different waveguide cross sections to study how the WG geometry affects the χ^2 .

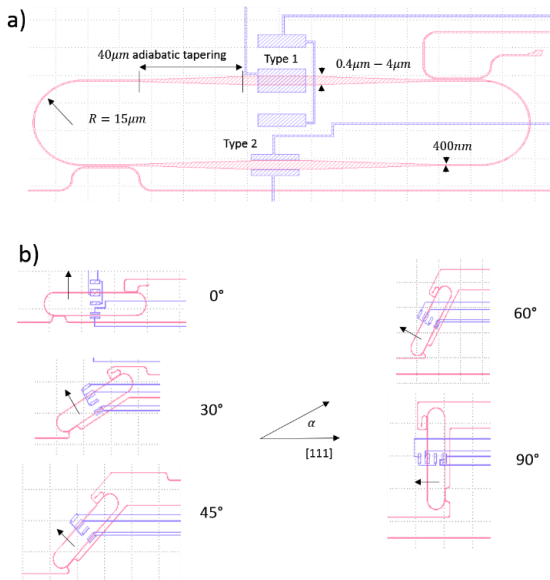


Figure 16. (a) Add-drop RTR's building blocks: optical layer (pink) and metal layer (violet). (b) Angled versions of the RTRs.

Figure 16(a) shows the building blocks of the RTR that is being used in add-drop configuration. The bends are mono-modal WG with a cross section of $400 \times 250 \text{ nm}$. There are adiabatic taperings, $40 \mu\text{m}$ long, to adapt the fundamental mode coming from the bends to the multimodal WGs located under the electric pads and to avoid higher order modes. The multimodal WG has a width that ranges from $0.4 \mu\text{m}$ to $4 \mu\text{m}$. As already introduced, there are 2 kind of electric pads, type 1, to apply a vertical electric field (out of the plane) and type 2, to apply an horizontal electric field (in plane). Figure 16(b) sketches the RTRs for several angle α : 0° - 30° - 45° - 60° - 90° .

The samples have been fabricated at FBK using SOI wafers with silicon thickness of 250 nm . Two different silicon nitride thickness has been used as stressing layer, 70 nm and 140 nm . Characterization is underway.

A collaboration with the Scuola Superiore Sant'Anna has been started with the aim to find a phenomenological relation between the strain tensor and the χ^2 tensor in the strained silicon subject. Infact, starting from the experimental data and the strain map, obtained using COMSOL, they can develop a model that allows to predict the χ^2 for any WG geometry. An example of simulated strain map is reported in figure 17.

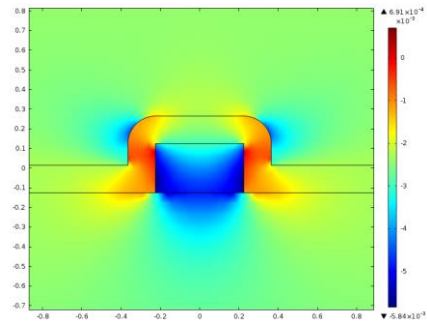


Figure 17. Simulated map of the exx (strain tensor) obtained by COMSOL. WG dimension $400 \times 250 \text{ nm}$, silicon nitride stressing layer 140 nm .

For more info

Nanoscience Laboratory
Department of Physics
University of Trento
via Sommarive 14
38123 Povo- Trento (Italy)
<http://nanolab.physics.unitn.it/>

secretary dr. Tatsiana Yatskevich
email tatsiana.yatskevich@unitn.it
phone +390 461 283172